The influence of thermal and visible light activation modes to the NO_2 response of electro-spun WO_3 nanofibers

L. Giancaterini, S.M. Emamjomeh, A. De Marcellis, E. Palange, A. Resmini[1], U. Anselmi-Tamburini[1], C. Cantalini

Department of Industrial and Information Engineering and Economics, Via G. Gronchi 18,

University of L'Aquila, I-67100 L'Aquila, Italy

Department of Chemistry, Via Taramelli 12 University of Pavia, I-27100, Pavia, Italy

* Corresponding author. Tel.: +39 0862 434233

E-mail address: carlo.cantalini@univaq.it (Prof. Carlo Cantalini)

Abstract

The influence of different visible light wavelenghts (Red λ=670nm, Green λ =550nm, and Purple-Blue λ =430nm), different light intensities (30 – 770 [μW/cm^2]), different operating temperatures (25 to 100°C) on the electrical response of WO3 electrospun nanofibers (NFs) to 100-400 ppb NO2 gas in dry air are here reported. WO3 NFs were prepared by mixing a W-O sol-gel transparent solution (WCl6 in ethanol) with a polymeric solution made of polyvinylpyrrolidone (PVP) and dimethylformamide (DMF). Electrospun NF were annealed between 300 and 500 °C and the microstructural features investigated by SEM and XRD techniques. Room temperature gas responses of the 450 °C annealed NFs has shown that with increasing both light wavelength and intensity, beside a slight decrease of the relative response, recovery of the base line and response times greatly improves as respect dark conditions. At operating temperatures ranging from 25 to 100°C, sensor relative responses in dark always resulted to over-perform the ones displayed under PB light. Light radiation, at low operating temperatures, resulted to powerfully enhance both recovery of the base

line and response times. By the combined action of Purple Blu light (λ = 430 nm) set at 770 [μW/cm2] intensity and by mild operating at 75°C operating temperature, relative responses (RRs) of 12.4, recovery percentages (RPs) of 97% of the base line were attained to 400 ppb NO2. The opportunity for tuning the response of WO3 NFs to NO2 via combined photo and mild thermal activation means is here addressed and discussed, considering the involved response mechanisms.

Keywords

Visible light, WO3; Nano fibers; gas sensors, room temperature

Highlights

- Room temperature influence of different visible light sources and different light intensities on the Relative-Response and Base-Line-Recovery to 400 ppb NO2 of WO3 NFs
- The influence of both Purple-Blu (PB) light and operating temperature (25-100 °C) on the NO2 response (100- 400 ppb)
- By the combined action of Purple Blu light (λ = 430 nm and 770 [μW/cm2]) and mild operating temperatures at 75°C, Relative Responses (RRs) of 12.4 and Recovery Percentages (RPs) of 97% of the base line were attained to 400 ppb NO2.
-

1. Introduction

Thermal activation mode at different operating temperatures (OT) represents up to date one of the most common strategy to increase the catalytic activity of metal oxides sensors (MOX) toward gas sensing. Regarding WO3 thin films, thermal activation mode at temperatures ranging from 150 °C to 200 °C has shown to substantially improve the NO2 and H2 gas relative response, to enhance the base line recovery and to decrease the adsorption/desorption times [1-2]. Drawbacks of the thermal activation mode are jet represented by power consumption and long term drift of the electrical signal related to diffusion and sintering effects at grain boundaries of polycrystalline MOX.

The need to decrease the OT, eventually to mild (<100 °C) or even room temperatures, has been recently achieved by the introduction of new preparation techniques yielding hierarachical WO3 [3]

or Pd loaded WO3 nanostructures [4]. Indeed an interesting alternative to thermal heating is actually represented by illuminating the sensitive MOX at low operating temperatures by means of UV or visible light sources, considering the photo catalytic response shown by some metal oxides. Room temperature illumination in the range 380-395 nm UV-light wavelenght of polycrystalline SnO2 and ZnO thin films [5-6], ZnO nanorods/tetrapods [7-8], TiO2 nanofibers [9], WO3 thick films [10-11], individual SnO2 [12] and SnO2-Core/ZnO-Shell nanowires [13] demonstrated surprisingly faster desorption times and enhanced base line recovery, providing means for new self cleaning capabilities. More recently improvements of the above mentioned gas response properties al low or mild temperatures have been also reported by utilizing visible light radiation at wavelengths ranging from purple (λ=400 nm) to red (λ=630 nm). Among them thin SnO2 [14], thick ZnO [15], mesoporous In_2O_3 and WO3 [16-17], thick WO_3 [11] played the major role. Aim of this paper is to discuss the influence of thermal and visible light-activated responses to sub ppm NO2 concentrations of 1D-WO3 policrystalline electrospun nanofibers (NF). Tests have been carried out at different visible wavelengths (480-630 nm), different operating temperatures (25–100 °C) and different light intensities (30- 770 μW/cm^2). Best operating conditions have been optimised considering sensors relative response, recovery of the base line and adsorption/desorption times as function of the incident visible light energy (eV) and intensity (μW/cm2). The NO2 gas responses are presented and compared to literature, explanations regarding the influence of both temperature and light on gas response are discussed in the light of the prevailing mechanisms.

2. Experimental

2.1 WO3 NFs preparation and microstructural characterization

The tungsten oxide nanofibers were fabricated by electro spinning method. All the chemicals in an analytical grade were purchased by Sigma-Aldrich. The WO_3 precursor solution was made by dissolving 0.4g of hexa-chlorotungsten-anhydrous (WCl6) in 5mL of ethanol in a glow box under N_2 controlled atmosphere (T = 29.2 °C, RH = 4.5 ± 2). WO3-Transparent precursor WO3-TR was

obtained after 3 days refluxing in N2 carrier gas. The evolution over time of the WO3 alkoxide peaks inside the precursor solution was monitored by FTIR technique (THERMO NICOLET NEXUS 870). The WO3-TR, after being kept idle for further 2 days to monitor the absence of precipitation phenomena, was mixed with a polymeric solution (PVP+DMF) previously prepared by dissolving 0.17g of polyvinylpyrrolidone (PVP MW = 1,300,000) in 1mL of dimethylformamide (DMF). The final solution (PVP+DMF) + (WO3-TR) was prepared in N2 controlled atmosphere by adding drop by drop the polymeric (PVP+DMF) to the precursor (WO3-TR) solution. Thermal stability and weight loss with temperature of the all the prepared solutions were investigated by Thermo-Gravimetric Analysis (TGA) technique using (LINSEIS L81-I) at a heating rate of 2 ˚C/min to up to 500 °C in static air. The final solution (PVP+DMF) + (WO3-TR) was electrospun in a glow box under N_2 controlled atmosphere (T = 29.2 °C, RH = 4.5 ± 2), by means of an home-made electro spinning apparatus consisting of: a plastic syringe equipped with 23SP Needle, microfluidic pump (LEGATO KD SCIENTIFIC 110), high voltage power supplier (ULTRAVOLT High Voltage Power Supply, range 0-30 kV), and a rotating collector provided with *x-y* position controller. Electrospinning of nano-fibers (NF) was done on a silicon nitride (Si_3N_4) substrate with front side Pt finger-type patterned electrodes and back-side heating circuit. The applied tension, distance and solution flow rate were set at: 14kV, 10 cm and 1µl/min, respectively. After spinning, NFs were oven-annealed in static air for 1 hour in the temperature range 300-500 °C temperatures with an heating and cooling rate of 2°C/min. Morphology, size and structure of the annealed WO3 NFs were recorded on FEG-SEM instrument (TESCAN MIRA 3 XMU Microscope). Crystalline phases evolution of the annealed at different temperatures was monitored by grazing incidence XRD (Philips XXX) with Cu Kα1 radiation (λ=0.154 nm) and 0.02° angle step.

2.2. WO3 NFs electrical characterization (De Marcellis)

The electrical resistance of the NFs to NO2 and H2 gas was measured by an automated system. NFs placed inside a Teflon chamber (500 cm^3), provided with Teflon tubings, were exposed to NO2 gaseous mixture (at 500 sccm/min flow rate) ranging from 20 to 400 ppb (NO2) in dry air. Different gas concentrations were obtained by mixing certified NO2 mixtures (5 ppm NO2 in dry air cylinder) with dry air carrier by means of an MKS147 multi gas mass controller. NO_2 gas concentrations in the down stream were measured by means of Ansyco AS32 M chemiluminescence analyser (Environment S.A). NFs electrical resistance was measured by means of a Volt-Amperometric technique (AGILENT 34970A) at different Operating Temperatures (OT) in the range 25 – 100 °C by heating the Si3N4 substrate thorough back-side-circuit *dc* current injections (20-80 mA). Electrical tests in the 25-100 °C OT range and different NO2 concentrations were recorded both in dark and by illuminating the NFs by means of different visible-light sources (Purple-Blu (PB) λ=430nm; Green (GR) λ=570nm; and Red (RD) λ=640 nm) utilizing commercial LED (Kingbright 10 mm full color RGB lamp-LF81WAEMBGMBC). Characteristic emission spectra of the LED sources have obtained by means of light monochromator. Different light intensities [μW/cm2] where utilized by changing the distances (from 0.5 to 3 cm) between LED sources and the surface of the films. Corresponding light intensities were measured by means of calibrated commercial power meter (Fieldmaster GS – Coherent Inc.) set at the central wavelength of each LED (Red=640nm; Green-=570nm ; Purple-Blue=430nm).

3. Results

3.1. W-O precursor-gel and NFs preparation and characterization

WO3 nanofiber production by electrospinning technique make use of a solution, here referred as the spinning solution (SPS) prepared by mixing a sol-gel precursor solution (SGP), containing the metal alkoxide, with a polimeric solution of high molecular weight (PMS). The spinning solution is then electrospinned to yield the “as-prepared” composite nanofibers bundle. Pure tungsten oxide

nanofibers are therefore obtained by removing the organic phase (PMS) via calcination of the "as-prepared" composite nanofibers in air. A large variety of precursor in combination with polimeric solutions have been successfully employed for the prepration of WO3 nanfibers as recently reported [18-22]. Among them we succeeded preparing the SGP solution using WCl6 dissolved in ethanol following the procedure reported [23], yielding a tungsten alkoxide $W(OC_2H_5)_6$ transparent chemically-stable SGP solution. In order to make the most effective use of the refluxing procedure to yield transparent SGP solution, we have monitored the evolution of W-O bonds inside the SGP solution by FTIR. Figure 1a shows the FTIR spectra of the SGP solution collected over a period of four days. Black plot has been taken after the first 1 hour, whereas red and blu refer to samples collected after 2 and 4 days refluxing respectively. From a qualitative point of view no differences can be found comparing the red and blu plots, corresponding to the SGP transparent solution collected after 2 and 4 days. It turns out that two days refluxing are at least needed to complete the stabilization of the chemical compounds inside the SGP transparent solution. On the other hand the large differences between the black plot, collected after 1 hour and the one after 2 days, provides strong evidence that the on set of the sol gel process has not jet activated after 1 hour. From a quantitave point of wiew apart from the broad band centered around 3370 cm^{-1} (OH stretching) and of the 1627 cm^{-1} (OH bending) showing the occurrence of W-alkoxides formation other peaks may be attributed to C=O and =CH2 bonds [24]. The on set of amorphous W-O bonds (shown in Fig. 1a) can be assigned, as shown in Fig. 1a and according to literature [24-25], to the shallow shoulder located at around 600 cm^{-1}. This W-O amorphous peak shifts towards higher wave numbers at 813 cm^{-1} (see green plot in Fig. 1a) in the 450 °C annealed WO3 electrospun nanofibers, and can be assigned to the formation of W-O-W crystalline bonds [25].

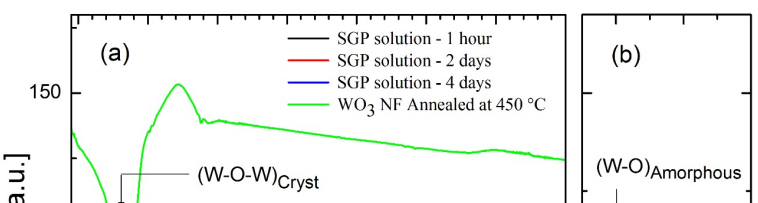

Fig. 1a survey FTIR spectra of the sol-gel precursor solution (SGP) collected after: 1 hour (Black), 2 (Red) and 4 days (blue) and the annealed WO3 NF at 450 °C (green). **Fig.1a** close-up in the FTIR 500 – 1000 cm^{-1} of the SGP solution

The spinning solution (SPS) prepared by mixing the sol-gel transparent precursor solution (SGP), with the polimeric solution (PMS), has been thermally characterized by thermogravimetric technique in the temeperature range 25-500°C in static air. **Fig. 2** shows the percentage of weight loss as function of temperature of the Polimeric (PMS) and the spinning solution (SPS) respectively.

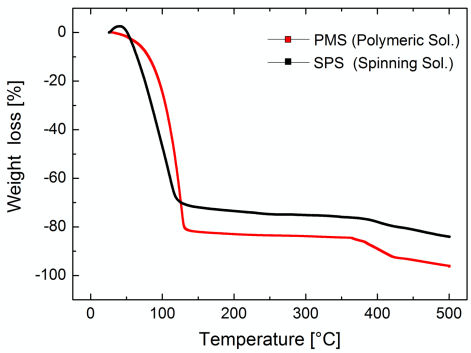

Fig. 2. Thermogravimetric p s function of temperature of the: polymeric solution (PMS – F ɔt)

The burn out of the PMS is almost completed at 150°C yielding an associated weight loss of 80 %. The 100% and 85% of full weight losses of the PMS and the SPS are respectively achieved in the temeprature range 450-500°C. These results imply that, besides the complete burn out of the PMS, the 15% of the SPS initial weight is still left at 500 °C. This 15% is in agreement with the calculated weight percentage of the expected WO3 in the Spinning solution after complete reaction of the WCl6 precursor and full crystallization. XRD diffraction measurements of the annealed at 400-450 and 500

°C are in line with previous research confirming the formation of monoclinic WO3 crystalline structure in the range 300-350 °C [1-2].

Fig. 3 compares the SEM immages of the as deposited and different temperatures annealed WO3 NF at low (left side) and high magnification (right side), deposited on Si3N4 substrates. From a morphological point of view there seems to be not a big difference comparing the as deposited NFs (Fig. 3a and 3b) with the 300°C annealed (Fig. 3c and 3d). Fibers at 300 °C still maintain a smooth appearance with lack of any sign of crystallization, confirming an incomplete removal of the polymer. Between 400 and 450 °C a sort of "spider web" structure is developed with entangled continuous fibers of rough surfaces made of loosely sintered grains as displayed in Fig.3e, f. At 450 °C fibers resulted to be shrinked as respect to the 300 °C, with diameters ranging from 20 to 100 nm and composed by a fine texture of micro-crystalline grains of around 20 nm size diameter. At 500 °C anneling, grain growth causes fibers to crack and the occurrence of extended fibers discontinuity as reported in Fig. 3g, h.

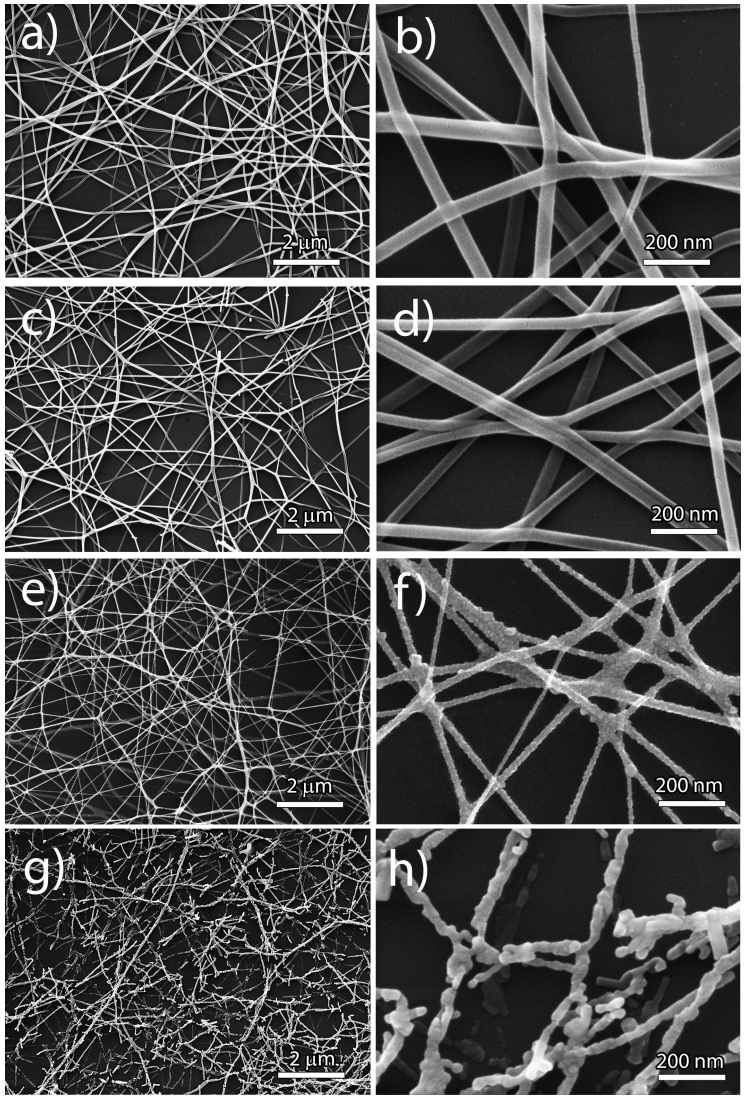

Fig. 3 SEM magnifications of electrospun nanofibers annealed at differente temperatures for 2 hour. (a +b) as deposited, (c+d) 300°C annealed, (e+f) 450°C annealed, (g+h) 500 °C annealed.

3.2 Electrical characterization

The gas response of MOX sensors activated by visible light sources is known to be dependant by its wavelength (nm) and intensity (W/cm2) respectively. A close characterization of the LED sources has been previously carried out before any gas response evaluation. **Fig. 4** display the normalized characteristic emission spectra of the commercial LED sources employed in this study, obtained by means of a light monochromator. LEDs main features confirmed peaks length located at λ=430nm Purple-Blu (PB), λ=570 nm Green (GR) and λ=640 nm (Red (RD) respectively and negligible overlapping of the emission spectra.

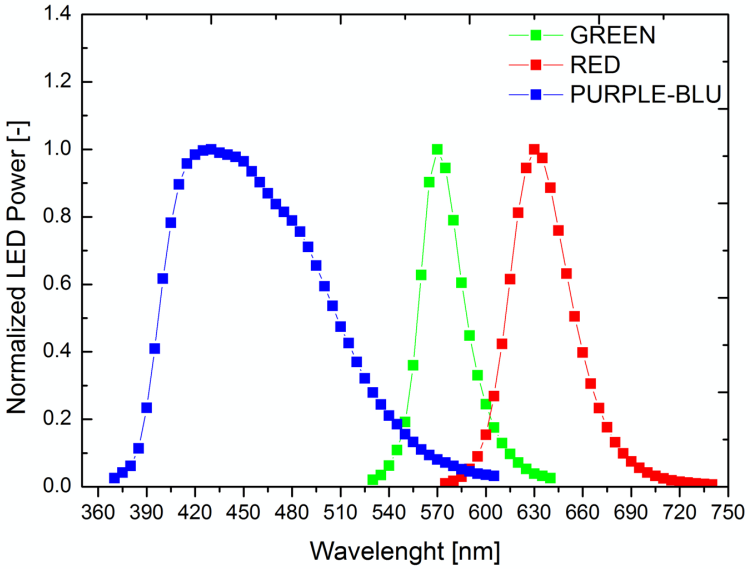

Fig. 4 Normalised LED powers characteristic emission spectra of the Purple-Blue, Green and Red measured by means of monochromator. Normalized LED power values are the integral of the LED spectral response

Light intensities [μW/cm2], computed by the integral of the LED emission spectra of Fig. 4, were calculated at four different distances (from 0.5 to 3 cm) between the LED sources and the light monochromator. LEDs visible light intensities are reported in table I.

LED	Light Intensity @ 0.5 cm [μW/cm^2]	Light Intensity @ 1cm [μW/cm^2]	Light Intensity @ 2cm [μW/cm^2]	Light Intensity @ 3cm [μW/cm^2]
RD-RED (640nm)	95	89	59	30
GR-GREEN (570nm)	40	38	27	15
PB-PURPLE BLUE (430nm)	770	668	468	270

Table I. LEDs intensities as a function of the distance from the power meter detector

Electrical gas responses have been carried out by exposing the 450 °C annealed WO3 NFs to a combined set of temperatures in the range (25-100°C) and by selecting the illumination between dark and light conditions corresponding to different wavelengths and intensities. Preliminary tests have been performed at room temperature (25 ± 2°C) to select the LED source which yield better "gas response properties". Figures of merit have been introduced to address these "gas response properties" in the way which follow:

- base line resistance (BLR): the resistance in dry air at equilibrium before a gas exposure
- relative response (RR): the ratio (R_G/R_A) or (R_A/R_G) for a given concentration of oxidizing or reducing gas respectively
- adsorption/desorption time ($\tau_{ads/des}$): the time required to reach 90% of the full response at equilibrium, both during adsorption and desorption
- recovery percentage (RP): the percentage ratio (Δ_D/Δ_A,) x 100, where Δ_D and Δ_A stand for the variation of the electrical resistance during adsorption and desorption respectively, calculated within the time scale of the sensing cycle (see Fig. 5 for its graphical representation)

Firstly it turns out that, given the time scale of a sensing cycle, adsorption/desorption times can be eventually numerically quantified only if equilibrium conditions are achieved. Secondly the recovery percentage (RP) is a measure of the sensor ability to regain, after degassing, its base line resistance (BLR). Under these circumstances it may be the case that by desorbing in air, equilibrium conditions are achieved (so that $\tau_{ads/des}$ can be quantified) but the sensor resistance fails to regain its original base line value. This apply in case of irreversible adsorption of gas molecules, bound so strongly to the surface that they never desorbs, regardless the time scale of a sensing cycle. Lastly it may be the case that no equilibrium conditions are achieved during desorption so that neither base line recovery is regained nor $\tau_{ads/des}$ times can be quantified.

Fig. 5 shows the influence of different visible light wavelengths on the gas response to 400 ppb NO2 at room temperature and dry air carrier gas. The time scale for each adsorption and desorption cycle has been set at 60 min. The distance of the LEDs sources from the sensor surface is placed at its minimum (0.5 cm). **Table II** display a quantitative description of the gas response features of the 450 °C annealed NFs.

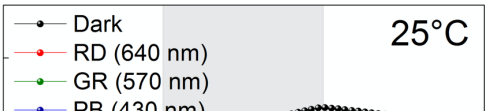

Fig. 5 The influence of different visible light wavelengths to 400 ppb NO2 at room temperature and dry air carrier gas, corresponding to a distance of the LEDs sources from the sensor surface of 0.5 cm

Light source	Wave lenght [nm]	Photon Energy [eV]	Intensity [μW/cm^2]	BLR [Ω]	RR [-]	RP [%]	τ_{ads} [min]	τ_{des} [min]
D-Dark	/	/	/	8.9 x 10^5	1.55±0.2	9	/	/
RD-Red	640	1.94	95	4.5 x 10^5	1.57±0.3	38	/	/
GR-Green	570	2.18	40	2.5 x 10^5	1.56±0.2	55	/	/
PB-Purple	430	2.88	270	1.4 x 10^5	1.49±0.2	83	/	/
			568	1.3 x 10^5	1.43±0.2	86	/	/
			770	1.2 x 10^5	1.38±0.2	92	/	/

Table II. Base line resistance (BLR), Relative Response (RR), Recovery Percentage (RP) and response times (τ_{ads}/τ_{des}) to 400ppb NO_2 at room temperature and different light wavelengths. Also reported sensor responses by changing the PB light intensities from 270 to 770 [μW/cm^2]

From Figure 5 and table II it turns out that with increasing light wavelenghts the base line resistance (BLR) decreases of almost one decade. Relative Responces (RR) are nearly constant under D, RD and GR radiation (i.e. 1.56±0.2), with the exception of the PB illuminated which decreases down to 1.38±0.2 at 770 [μW/cm2] intensity. Recovery percentages (RPs) remarkably improve from 9% (D) to 92% (PB). Considering the features and shapes of the plots displayed in Fig. 5 no ads/des equilibrium conditions were achieved within the time scale of the experiment. This is the reason why $\tau_{ads/des}$ times have not been shown in Table II.

The influence of the PB light intensity, which represents the energy flow rate [eV/s] of the impinging photons per unit area, obtained by changing the LED distances from sensor surface, is shown in Fig. 6. Numerical values are also reported in the last three lines of table II. Adsorption desorption times have been extended to a time scale of 3 hours to enhance equilibrium; sensor surface temperature has been controlled by a thermocouple positioned on the back side of the substrate. No local heating of the substrate corresponding to the highest intensity of 770 [μW/cm2] of the PB radiation was recorded Regardless its intensity, PB radiation decreases/increases (RRs)/(RPs) as compared to D, RD and GR lights. In detail by increasing PB light intensity the RRs slightly but steadily decrease (from 1.49 to 1.38) whereas RPs improve (from 83 to 92%). Equilibrium conditions are almost achieved during adsorption after three hours exposure to 400 ppb NO2. No equilibrium conditions were achieved during desorption in dry air within the time scale of the experiment.

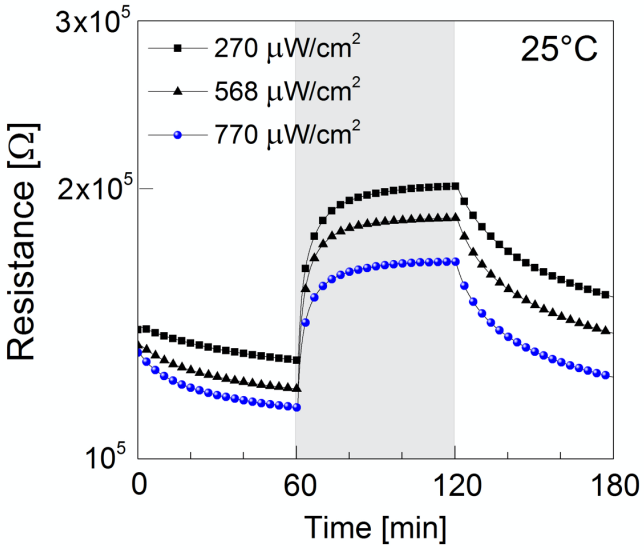

Fig. 6 The influence of different PB light intensities to 400 ppb NO2 at room temperature and dry air carrier gas. Light intensities have been measured by means of a monochromator by changing the distances between the LEDs source and the sensor surface.

PB light at 770 [μW/cm2]), although less responsive in terms of RRs, has been selected for further investigations, considering its superior recovery and faster response, in light of its practical application.

The influence of thermal and PB light activation modes to different NO2 sub-ppm concentrations are compared in **Fig. 7**. During the test PB light intensity was set at 770 [μW/cm^2] and the Operating Temperatures (OT) changed from 25 to 100 °C. Table III compares Relative Responses (RRs), Recovery Percentages (RPs) and response times (τ_{ads}/τ_{des}) as function of temperature, light and dark conditions. From Fig. 7 it turns out that the base line resistance, as represented by the dotted lines displayed in figure 7a, turns to an horizontal slope with increasing OT. This feature is well represented in Table III by the increase of the Recovery Percentages (RPs). To this extend the positive effect of light radiation is remarkable considering that RPs values under PB light reach so far 92% at 25°C, heading 99% at 100 °C as compared to 9% and 96% in dark respectively. Equilirium conditions during adsorption and desorption are hardly achieved starting from 75°C OT, considering 60 minutes the time scale of each cycle. Adsorption desorption times at equilibrium are slightly shorter under PB light radiation, but with a tendence to be comparable with one yielded in dark at 100 °C. Relative Responses under dark conditions are always greater than the one recorded under PB radiation thorought the 25-100 °C OT range. The bigger improvement of the relative response is displayed at 75 °C for both dark and light conditions, whereas a pronounced reduction of the RRs is recorded at 100 °C OT.

It may be concluded firstly that light activation mode decreases the base line resistance with decreasing light wavelenghts. Secondly that PB radiation slightly decrease the relative response (RR) as respect to D, GR and RD, and that RR further decrease by increasing PB light intensity. Thirdly that PB light source is the most effective to enhance the recovery percentage of the base line and to shorten ads/des times. Lastly the combined action of temperature and PB light demonstrated that by heaheating at 75°C and setting the PB light intensity at 770 [μW/cm^2] a relative response of 12.4 to 400 ppb NO2 and 97% recovery percentage of the base line is achieved.

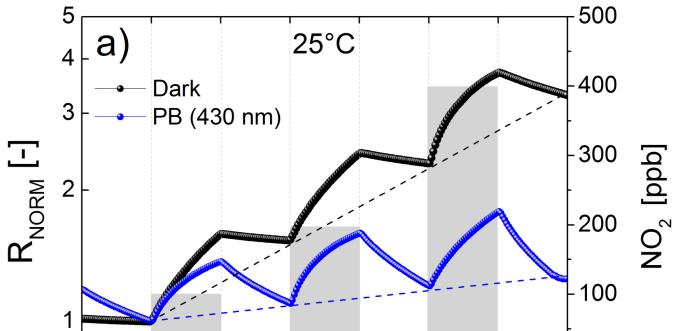

Fig. 7 Dynamic normalized responses of the 450 °C annealed WO3-NFs to NO2 gas (100 – 400 ppb in dry air) in Dark (black line) and Purple-Blue light (λ=430nm and 770 [μW/cm^2]) at different operating temperatures (25 – 100 °C)

	DARK CONDITION					PURPLE BLUE LIGHTING CONDITION				
Temperature [°C]	BLR [Ω]	RR=R_G/R_A [-]	RP $(\Delta_D/\Delta_A)*100$ [%]	τ_{ads} [*min*]	τ_{des} [*min*]	BLR [Ω]	RR=R_G/R_A [-]	RP $(\Delta_D/\Delta_A)*100$ [%]	τ_{ads} [*min*]	τ_{des} [*min*]
25	8.9 x 10^5	1.55	9	/	/	1.2 x 10^5	1.38	92	/	/
50	9.7 x 10^4	8.29	81	/	/	5.8 x 10^4	7.62	95	/	/

75	3.2 x 10^4	18.42	93	38	42	9.3 x 10^3	12.46	97	33	38
100	6.2 x 10^3	4.95	96	31	33	3.4 x 10^3	4.32	99	30	32

Table III. Comparison of the Relative Response (RR), Recovery Percentage (RP) and response times (τ_{ads}/τ_{des}) to 400ppb NO2 in Dark and PB light (λ=430nm and 770 [μW/cm^2]) at different operating temperatures (25 – 100 °C)

4. Discussion of the electrical response

4.1 Response in dry air

WO_3 is an off-stoichiometric oxide displacing a slight deficiency of lattice oxygen ions [WO_{3-x}] giving the structure its characteristic *n*-type behavior [1,26]. In air at equilibrium, ambient oxygen adsorb in the forms O_2^-, O^- or O^{2-}, depending on the surface temperature [27]. In the temperature range 25 – 100 °C, O_2^- is reported to be the most stable species, adsorbing primarily on lattice oxygen vacancies, according to reaction (1).

$$O_2 + V_O^{\bullet\bullet} + e_{CB}^- = \quad (O_2^- - V_O^{\bullet\bullet})_{ADS} \qquad (1)$$

where e_{CB}^- denotes electrons from the conduction band, $V_{\ddot{O}}$, according to the Kröger-Vink notation, represents a doubly charged positive oxygen vacancy and $(O_2^- - V_O^{\bullet\bullet})_{ADS}$ a chemisorbed oxygen coupled with $V_{\ddot{O}}$. This situation corresponds to the initial state of the WO3 NFs surface at equilibrium in ambient air.

At room temperature, by exposing to visible light , WO3 NFs behave in a similar way as previously extensively reported for thick [10,11] and mesoporous WO3 films [17]. The decrease of the base line resistances of Fig. 5 and Fig. 6 has been explained taking into consideration the photo-desorption of the adsorbed surface oxygen species $(O_2^- - V_O^{\bullet\bullet})_{ADS}$, induced by impinging photons with associated visible light energies ranging from 2.88 eV (PB) to 1.94 eV (RD). To this extend WO3 with a band gap of 2.75 eV [28], is a promising material since capable of desorbing O_2^- both by electronic band-to-band transition at λ ≤ 430 nm (first mechanism) and by direct adsorption of the incident photon by use of less energetic sources at λ ≤ 630 nm (second mechanism).

The first mechanism [6,10-11,15,17], as shown in the reactions which follow, occurrs at λ ≤ 430 nm (i.e. PB light @2.88 eV). Here the photo induced electron–hole couple (2) yields h^+ to desorb oxygen from $(O_2^- - V_O^{\bullet\bullet})_{ADS}$ (3) providing, at the same time, photo generated electrons ($e_{h\nu}^-$) with enough energy to overcome the band gap (located @ 2.75eV), which quickly recombine with $O_{2(g)}$ (4). A new equilibrium is thus displaced (5), comprising the presence of strongly chemisorbed $(O_2^- - V_O^{\bullet\bullet})_{ADS}$ and lessen bounded $(O_2^- - V_O^{\bullet\bullet})_{h\nu}$. Based on this, oxygen on the whole is not desorbed from the surface, but is actually, partially transformed, to a less electro-negative $(O_2^- - V_O^{\bullet\bullet})_{h\nu}$ species which is responsive for the thinning of the depletion layer and eventually for the decrease of the base line resistance as displayed in fig. 5.

$$h\nu \rightleftharpoons e^- + h^+ \qquad (2)$$

$$(O_2^- - V_O^{\bullet\bullet})_{ADS} + h^+ \rightleftharpoons O_{2(g)} + V_O^{\bullet\bullet} \qquad (3)$$

$$O_{2(g)} + V_O^{\bullet\bullet} + e_{h\nu}^- \rightleftharpoons (O_2^- - V_O^{\bullet\bullet})_{h\nu} \qquad (4)$$

$$\left(O_2^- - V_O^{\square\square}\right)_{ADS} \rightleftharpoons \left(O_2^- - V_O^{\square\square}\right)_{h\nu} \qquad (3 + 4) = (5)$$

To this extend, the slightly decrease of the base line resistance of Fig. 6 with the increase of the PB light intensity (from 270 to 770 [μW/cm2]), may be attributed to a shift of the equilibrium of reaction (5) to the right, enabling the increase of the concentration of further lessen charged states.

The second mechanism takes place by direct impingement of photons ($h\nu$) on to $(O_2^- - V_O^{\bullet\bullet})_{ADS}$, enabling direct desorption of adsorbed oxygen according to reaction (6)

$$(O_2^- - V_O^{\bullet\bullet})_{ADS} + h\nu \rightleftharpoons O_{2(g)} + V_O^{\bullet\bullet} + e \qquad (6)$$

Less energy of the impinging photon is required for reaction (6) to occur, considering that the binding energy of chemically-adsorbed oxygen atoms on defective SnO2, has been estimated to be 1.67 eV [29]. To this extend, as shown in fig. 5, Red (RD @ λ = 630 nm) and Green (GR @ λ = 570 nm) lights with associated energies of 1.94 and 2.18 eV respectively are, so far, suitable to activate the second mechanism, therefore contributing to the decrease of the base line resistance. It turns out that both the two mechanisms contribute to oxygen desorption but with significant differences in terms of

base line recovery and adsorption/desorption times. The bigger recovery percentages (RPs) of the PB as respect to RD and GR lights illuminated samples, as shown in table II and Fig. 5, are explained considering that PB light trigger interband fast electrons transition, whereas RD and GR lights activate only surface desorption processes, with longer timescales, characteristic of chemical desorption process at room temperature.

4.1 Response to NO2

Preliminary studies on NO_2 gas molecules adsorption on SnO_{2-x} defective metal oxide surfaces highlighted that at temperatures T< 200 °C, NO2 molecules primarily adsorbs on surface oxygen vacancies $V_O^{\bullet\bullet}$ [30-32]. Considering the stronger attitude of NO2 as respect to O2 to extract electrons, two adsorption mechanisms have been tentatively proposed which explain the increase of the electrical resistance of *n*-type materials like WO3, when exposed to few ppm NO2 [33].

At room temperature and dark condition, a surface electron transfer mechanism takes place (7), whereas at higher temperatures a thermally-activated transition of bulk-generated conduction band electrons (e_{CB}^-) prevails (8).

$$NO_{2(g)} + (O_2^- - V_O^{\bullet\bullet})_{ADS} \rightleftharpoons (NO_2^- - V_O^{\bullet\bullet})_{ADS} + O_{2(g)} \quad (7)$$

$$NO_{2(g)} + V_O^{\bullet\bullet} + e_{CB}^- \rightleftharpoons (NO_2^- - V_O^{\bullet\bullet})_{ADS} \quad (8)$$

At room temperature and PB light radiation the oxide surface is characterised by the presence of $(O_2^- - V_O^{\bullet\bullet})_{ADS}$ in equilibrium with $(O_2^- - V_O^{\bullet\bullet})_{h\nu}$ (see reaction 5). In this case NO2 molecules are expected to react as proposed by reactions (7) and (9)

$$\begin{array}{lll} & (O_2^- - V_O^{\bullet\bullet})_{ADS} \rightleftharpoons (NO_2^- - V_O^{\bullet\bullet})_{ADS} + O_{2(g)} & (7) \\ NO_{2(g)} & \uparrow\downarrow & \\ & (O_2^- - V_O^{\bullet\bullet})_{h\nu} \rightleftharpoons (NO_2^- - V_O^{\bullet\bullet})_{h\nu} + O_{2(g)} & (9) \end{array}$$

According to (7) and (9), the smaller increase of the resistance at room temperature of the PB illuminated WO3 as respect to samples in dark (table II, Fig. 5 and Fig. 7a), may be explained considering firstly, that the depth of the depletion layer always increases by NO2 adsorption, secondly

that the increase occurs, by contrast, to different extents. Indeed, under light, the circumstance of a pre-existing thinner depletion layer associated with the formation of less charged $(O_2^- - V_O^{\bullet\bullet})_{h\nu}$, eventually inhibit the formation of larger depleted zones after NO2 adsorption. This has been represented by reaction (9) considering the formation of $(NO_2^- - V_O^{\bullet\bullet})_{h\nu}$ adsorbates, with associated reduced surface charge. It turns out that under NO2 gas, PB radiation decreases the Schottky barrier height between the grains, giving rise to a smaller increase of the sensor resitance, thus explaining the smaller RRs of the illuminated as respect to dark samples. Moreover the reduced RRs to NO2, by increasing PB light intensities (see fig. 6 and table II) could be also explained taking into consideration that equilibrium of reaction (5) could shift to the right, giving rise to a larger amount of $(NO_2^- - V_O^{\bullet\bullet})_{h\nu}$adsorbates when exposing the surface to NO2. Eventually, at room temperature, the better recovery percentages (RPs) of the illuminated samples after degassing, may account also for an easier desorption process of lessen bounded $(NO_2^- - V_O^{\bullet\bullet})_{h\nu}$ species as respect to the more strongly charged $(NO_2^- - V_O^{\bullet\bullet})_{ADS}$.

Finally by increasing the operating temperature under dark conditions, the formation of thermally activated conduction bands electrons enables reaction (8) to suceed as respect to reaction (7). The occurrence of reaction (8) alone, (since reactions (7) and (9) are excluded in dark), explains the bigger resistance increase to NO2, with a maximum of the relative response at 75°C. The poor recovery of the base line by degassing at temperatures < 50°C (see black plot of Fig. 7a and 7b) could be also explained considering that thermal desorption of strongly charged $(NO_2^- - V_O^{\bullet\bullet})_{ADS}$ species is reported to starts at around 80 °C [31].

By increasing the operating temperature under PB light radiation, the adsorption of NO2 molecule takes place by way of both reaction (8) and reaction (9). The latter, as previously discussed, partially inhibits the resistance increase, due to the formation of a thinner depletion layer. From these premises it turns out that the NO2 gas resistance changes, under PB light, are always smaller as respect the one displaced in dark (compare dark and blu plots of Fig. 7). It should also be pointed out that thermal

activation mode is more effective to boost electrical changes as respect to light activation. Considering the porous nature of the NFs, made of poorly sintered grains, thermal heating switch on the whole material surface to react to NO2, whereas under PB light, only the illuminated photon-impinged surfaces, partecipate to the overall response.

Conclusions

The influence of thermal and visible light activation modes of electrospun WO_3 nanofibers annealed at 450 °C has been presented with the aim to investigate the influence of different visible-light wavelengths, intensities, operating temperatures and their combined effects, on to the NO2 gas responses in the concentration range 100 – 400 ppb. Room temperature gas responses of the 450 °C annealed NFs has shown that with increasing both light wavelength and intensity, beside a slight decrease of the relative response, recovery of the base line and response times greatly improves as respect dark conditions. Sensor relative responses to NO2 gas in dark resulted always to over perform the one recorded under PB light, in the investigated temperature range 25-100°C. This behavior has been explained considering the formation of less charged surface species arising from PB radiation of the WO3 surfaces. Indeed we found that light radiation powerfully enhances almost the full recovery of the base line, and faster response times at low operating temperatures. This paper highlighted also that by the combined action of Purple Blu light (λ = 430 nm) with beam intensity as low as 770 [μW/cm2]) and mild operating temperatures at 75°C, relative responses of approximately RR= 12.4 and almost the 97% of the full recovery of the base line were achieved by exposing the WO3 NFs to 400 ppb NO2. This paper address the big opportunity for tuning the response of WO3 NFs to NO2 via combined photo and mild thermal activation means.

References.

[1] C. Cantalini, L. Lozzi, M. Passacantando, S. Santucci, The comparative effect of two different annealing temperatures and times on the sensitivity and long term stability of WO_3 thin films

for detecting NO_2, IEEE Sens. J. 3 [2] (2003) 171-179

[2] A. De Marcellis, G. Ferri, P. Mantenuto, L. Giancaterini, C. Cantalini WO3 Hydrogen Resistive Gas Sensor and its Wide-Range Current-mode Electronic Read out circuit, , IEEE Sensor Journal, 13 [7] (2013) 2792 – 2798

[3] C. Wang, R. Sun, X. Li, Y. Sun. P. Sun, F. Liu, G. Lu, Hierarachical flower-like WO3 nanostructures and their gas sensing properties, Sens. & Act. B 204 (2014) 224-230

[4] B. Liu, D. Cai, Y. Liu, D. Wang, L. Wang, Y. Wang, H. Li, Q. Li, T. Wang, Improved room-temperature sensing performance of directly formed Pd/WO3 nanocomposite, Sens. & Act. B 204 (2014) 224-230

[5] E. Comini, G. Faglia, G. Sberveglieri, UV light activation of Tin oxide thin filn for NO2 sensing at low temperatures, Sens. & Act. B 78 (2001) 73-77

[6] S.W. Fan, A. K. Srivastava, V. Dravid, UV-activated room-temperature gas sensing mechanism of polycrystalline ZnO, Appl. Phys.Lett. 95 (2009) 142106-1421106-3

[7] G. Lu, J. Xu, J. Sun, Y Yu, Y.Zhang, F. Liu, UV-enhanced room temperature NO2 sensor using ZnO nonorods modified with SnO2 nanoparticles, Sens. & Act. B 162 (2012) 82-88

[8] O. Lupan, L.Chow, G. Chai, A single tetrapod-based sensor, Sens. & Act. B 141 (2009) 511-517

[9] E. Zampetti, A. Macagnano, A. Bearzotti, Gas sensor based on photoconductive electrospun titania nanofibres operating at room temperature, J. Nanoparticle Res. 15 (2013) 1566

[10] A. Giberti, C. Malagu', V. Guidi, WO3 sensing properties enhanced by UV illumination: An evidence of surface effect, Sens. & Act. B 165 (2012) 59-61

[11] C. Zhang, A. Boudiba, P De Marco, R. Snyders, M.G. Olivier, M. Debliquy, Room temperature responses of visible-light illuminated WO3 sensors to NO2 in sub-ppm range, Sens. & Act. B 181 (2013) 395-401.

[12] J.D. Prades, R. Jimenez-Diaz, F. Hernandez-Ramirez, S. Barth, A. Cirera, A. Romano-Rodriguez, S. Mathur, J.R. Morante, Equivalence between thermal and room temperature UV light-modulated responses of gas sensors based on individual SnO2 nanowires, Sensors and Actuators B 140 (2009) 337–341

[13] S. Park, S. An, Y. Mun, and C. Lee, UV-Enhanced NO2 Gas Sensing Properties of SnO2-Core/ZnO-Shell Nanowires at Room Temperature, ACS Appl. Mater. Interfaces 5 (2013) 4285−429

[14] K. Anothainart, M. Burgmair, A. Karthigeyan, M. Zimmer, I. Eisele, Light enhanced NO2 gas sensing with tin oxide at room temperature: conductance and work function measurements, Sens. & Act. B 93 (2003) 580-584

[15] Q. Geng, Z. He, X. Chen, W. Dai, X. Wang, Gas sensing property of ZnO under visible light irradiation at room temperature, Sens. & Act. B 188 (2013) 293-297

[16] D. Klaus, D. Klawinski, S. Amrehn, M. Tiemann, T. Wagner, Light activated resistive ozone sensing at room temperature utilizing nanoporous In2O3 particles: Influence of particle size, Sens. & Act. B 217 (2015) 181-185

[17] L. Deng, X. Ding, D. Zeng, S. Tian, H. Li, C. Xie, Visible light activated mesoporous WO3 sensors with enhanced formaldeyde-sensing property at room temperature, Sens. & Act. B 163 (2012) 260 – 266

[18] J. Y. Leng, X.-J. Xu, N. Lv, H. T. Fan, T. Zhang, Synthesis and gas-sensing characteristics of WO3 nanofibers via electrospinning, J. Colloid Interface Sci., 356 (2011) 54–57.

[19] G. Wang, Y. Ji, X. Huang, X. Yang, P. I. Gouma, M. Dudley, Fabrication and Characterization of Polycrystalline WO3 Nanofibers and Their Application for Ammonia Sensing, *J. Phys. Chem. B 110 (2006)* 23777-23782

[20] H. S. Shim, J. W. Kim, Y.E. Sung, W.B. Kim, Electrochromic properties of tungsten oxide nanowires fabricated by electrospinning method, Solar Energy Mat & Solar Cells 93 (2009) 2062-2068

[21] T. A. Nguyen, T. S. Jun, M. Rashid, Y. S. Kim, Synthesis of mesoporous tungsten oxide nanofibers using the electrospinning method, Mater. Lett. 65 (2011) 2823–2825

[22] T. A. Nguyen, S. Park, J. B. Kim, T. K. Kim, G. H. Seong, J. Choo, Y. S. Kim, Polycrystalline tungsten oxide nanofibers for gas-sensing applications, Sensors and Actuators B 160 (2011) 549– 554

[23] K. Nishio, T. Set T. Tsuchiya, Preparation of Electrochromic Tungsten Oxide Thin Film by Sol-Gel Process, J. Ceram. Soc. Jpn., 107 [3] (1999) 199-203

[24] S. Badilescu, P.V. Ashrit, Study of sol–gel prepared nanostructured WO3 thin films and composites for electrochromic applications, Solid State Ionics 158 (2003) 187-197

[25] N. Prabhu, S. Agilan, N. Muthukumarasamy, C. K. Senthilukumaran, Effect of temperature an the structural and optical properties of WO3 nanoparticles prepared by solvo thermal method, Digest journal of Nanomaterials and Biostructures 8 [4] (2013) 1483 - 1490

[26] P. Kofstad, Non-Stoichiometric, Diffusion and Electrical Conductivity in Binary Metal Oxides, Wiley, New York, 1972.

[27] S.C. Chang, Oxygen chemisorption on tin oxide: correlation between electrical conductivity and EPR measurements, J. Vac. Sci. Technol. 17 (1980) 366–369.

[28] P. P. González-Borrero, F. Sato, A. N. Medina, M. L. Baesso, A. C. Bento, G. Baldissera, C. Persson, G. A. Niklasson, C. G. Granqvist, and A. Ferreira da Silva, Optical band-gap determination of nanostructured WO3 film, Appl. Phys.Lett. 96 (2010) 061909-061909-3

[29] A. Maiti, J.A. Rodriguez, M. Law, P. Kung, J.R. McKinney, P. Yang, SnO2 nanoribbons as NO2 sensors: insights from First Principles calculations, Nano Lett. 3 [8] (2003) 1025-1028

[30] B. Ruhland, T. Becker, G. Muller, Gas-kinetic interactions of nitrous oxides with SnO 2

surfaces, Sens. & Act. B 50 (1998) 85–94

[31] J.D. Prades, A. Cirera, J.R. Morante, J.M. Pruneda, P. Ordejon, Ab initio study of NOx compounds adsorption on SnO2 surface, Sens. & Act. B 126 (2007) 62–67

[32] M. Batzill, U. Diebold, The surface and materials science of tin oxide, Prog. Surf. Sci. 79 (2005) 47–154

[33] M.J. Madou, S.R. Morrison, Chemical Sensing with Solid State Devices, AcademicPress, San Diego, 1989